JCTC Journal of Chemical Theory and Computation

Quantum Chemical Calculations of the Influence of Anchor-Cum-Spacer Groups on Femtosecond Electron Transfer Times in Dye-Sensitized Semiconductor Nanocrystals

P. Persson,*[,†,‡] M. J. Lundqvist,[†] R. Ernstorfer,[§] W. A. Goddard III,[‡] and F. Willig[§]

Department of Quantum Chemistry, Uppsala University, Box 518, SE-751 20 Uppsala, Sweden, Materials and Process Simulation Center, Beckman Institute 13974, California Institute of Technology, Pasadena, California 91125, and Hahn-Meitner-Institut, Glienickerstrasse 100, D-14109 Berlin, Germany

Received June 2, 2005

Abstract: Electronic properties of dye-sensitized semiconductor nanocrystals, consisting of perylene (Pe) chromophores attached to 2 nm TiO_2 nanocrystals via different anchor-cum-spacer groups, have been studied theoretically using density functional theory (DFT) cluster calculations. Approximate effective electronic coupling strengths for the heterogeneous electron-transfer interaction have been extracted from the calculated electronic structures and are used to estimate femtosecond electron-transfer times theoretically. Results are presented for perylenes attached to the TiO_2 via formic acid (Pe−COOH), propionic acid (Pe−CH_2−CH_2−COOH), and acrylic acid (Pe−CH═CH−COOH). The calculated electron transfer times are between 5 and 10 fs with the formic acid and the conjugated acrylic acid bridges and about 35 fs with the saturated propionic acid bridge. The calculated electron injection times are of the same order of magnitude as the corresponding experimental values and qualitatively follow the experimental trend with respect to the influence of the different substitutions on the injection times.

1. Introduction

Light excitation of dye molecules that are chemically bound to a semiconductor electrode can lead to heterogeneous electron transfer from the dye to the semiconductor if the excited state of the dye overlaps the semiconductor conduction band energetically.[1,2] The realization that such photoinduced heterogeneous electron transfer constitutes a highly efficient way to achieve charge separation has paved the way for the development of so-called dye-sensitized solar cells.[3,4] The introduction of nanocrystalline titanium dioxide (TiO_2) electrodes by Grätzel and co-workers meant that high device efficiencies could be achieved by taking advantage of its spongelike morphology giving up to a 1000-fold increase in photoactive surface area compared to traditional flat electrodes.[5] Thousands of organic and organometallic dyes have by now been tested in order to optimize the device efficiency.[6]

The desire to design more efficient devices has also spurred considerable interest in the nature of the ultrafast heterogeneous electron-transfer processes itself, with the hope that better control of the interfacial electronic properties will help to develop better devices.[1] The basic structural and electronic properties of a typical interface are illustrated in Figure 1. To ensure long-term stability of the interfaces, the chromophores are functionalized by special anchor groups, such as carboxylate and phosphonate groups, which are capable of forming strong chemical bonds to the semiconductor electrodes.[6] The electronic contact between the chromophore and the semiconductor can be controlled by insertion of so-called spacer groups between the chromophore and the anchor group.[7] The typical photoinduced charge separation is initiated by light excitation of the dye from its

* Corresponding author e-mail: petter.persson@kvac.uu.se.
[†] Uppsala University.
[‡] California Institute of Technology.
[§] Hahn-Meitner-Institut.

10.1021/ct050141x CCC: $33.50
Published on Web 01/10/2006

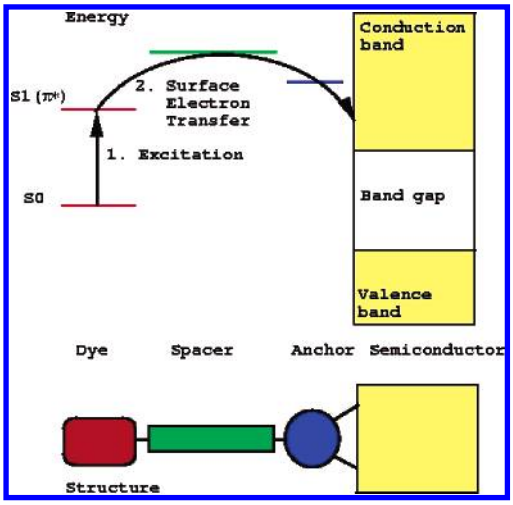

Figure 1. Schematic illustration of the relationship between the molecular structure and the electronic properties of photoinduced heterogeneous electron transfer processes, in dye-sensitized semiconductor devices. The upper and lower panels show the electronic and structural interactions of the various components, respectively. The chromophore part of the dye is attached to the semiconductor via spacer and anchor groups. The photoinduced heterogeneous electron transfer process typically occurs in a two-step process (upper panel), where there is first a local photoexcitation of the dye, followed by surface electron transfer across the spacer-cum-anchor bridge to the semiconductor conduction band which provides a quasi-continuum of electron acceptor states.

electronic ground state to an excited electronic state that is located above the conduction band edge of the semiconductor energetically. The electron injection rate depends strongly on the ability of the anchor-cum-spacer unit that separates the dye from the semiconductor to mediate the electron transfer. In the fastest possible electron transfer processes, the group that anchors the molecule to the semiconductor can act as an efficient conduit of electron transfer by effectively removing the tunneling barrier to the heterogeneous electron transfer.[8]

Ultrafast pump−probe laser spectroscopy has been used extensively to determine electron transfer rates for a number of dye-semiconductor systems with increasingly high time resolution, and it has been shown that electron transfer takes place on a femtosecond time scale in many dye-semiconductor systems.[9−12] The extremely rapid injection rates for a wide range of donors distinguish the heterogeneous electron-transfer processes from most long-range homogeneous, molecular, and biological electron-transfer processes.[13] The enhanced rates for heterogeneous electron transfer are largely caused by the presence of a band of acceptor states offered by the semiconductor substrate, as opposed to the single acceptor state encountered in purely molecular systems, for as long as the donor state lies above the conduction band edge it remains in resonance with a number of acceptor levels.[14] In this situation the electron transfer rate becomes less dependent on vibrational activation compared to most molecular electron transfer reactions that follow the Marcus electron transfer model in which the electron transfer takes place only when the vibrational motion in the donor state reaches a crossing point with the acceptor state where the electronic levels of reactants and products become isoenergetic.[15] The rate of electron transfer is in the heterogeneous case instead largely determined by the strength of the electronic coupling between the excited state of the dye and the semiconductor conduction band. Moreover, the electron transfer in these systems can under favorable conditions take place prior to thermal equilibration of the excited donor state,[16] in contrast to earlier assumptions.[17]

Theoretically, intramolecular and homogeneous electron-transfer processes have been studied extensively.[13,18] Photoinduced heterogeneous electron transfer of dye-sensitized nanoparticles is much less well understood, despite its significant technological potential.[19] Theoretical studies focusing on the conceptual understanding of various aspects of the heterogeneous electron-transfer processes have been presented in the last years.[20,21] The complexity of dye-sensitized semiconductors has, on the other hand, limited the possibilities of quantum chemical calculations and simulations that can provide the predictive power associated with methods that do not rely on fitted parameters.[22] Quantum chemical calculations have been used to investigate the structural and electronic factors involved in the binding of Ru-dye ligands to TiO_2 surfaces as well as studies of the nature of photoinduced electron transfer and charge-transfer excitations of various sensitizers on TiO_2 nanoparticles.[22−35] These studies have, for example, shown that it is important to take both the physical and electronic structure of the interface into account, to model the interface behavior accurately. Structurally, the adsorption can cause significant distortions of the adsorbate structure to accommodate the most favorable surface binding.[22,23] Electronically, the adsorption induces changes in the electronic structure of the adsorbate, in particular in the anchor group.[22,25] Also, the ability to study femtosecond electron-transfer processes from dye molecules to TiO_2 surfaces, either from an electronic coupling,[27,33] a nonadiabatic molecular dynamics,[28] or an electron dynamics[30] perspective, has been explored. The inclusion of nuclear motion in the nonadiabatic molecular dynamics approach makes it particularly attractive for cases where the electronic coupling varies significantly as a result of the motion of the nuclear positions, e.g. due to molecular vibrations.[28]

As reviewed by Noguera, there have been numerous theoretical studies of titanium oxide clusters,[36] including e.g. early work by Bredow and Jug on large TiO_2 anatase particles.[37] To explicitly account for the complexity encountered by using nanocrystalline TiO_2 electrodes, we have also recently made a more systematic computational investigation of small TiO_2 nanocrystals.[38] This approach makes it possible to investigate dye-sensitized TiO_2 nanocrystals using first principles DFT methods.[26,32,33] A potential problem with finite clusters is that they can have poorly developed band structures if they are too small, with e.g. an unphysically large finite level spacing in the substrate bands compared to the experimental situation. Here we use a model TiO_2 nanocrystal with 2 nm diameter which ensures that the splitting of the electronic levels in the relevant part of the conduction band is of the order of 10−20 meV. This spacing

provides an effective lower limit on observable coupling strengths for the dye-semiconductor interaction. A second frequent objection against using clusters as surface models is termination problems requiring the use of surrounding point charges or saturators. In the case of nanocrystals, however, a realistic description of the system may well require the presence of various types of surface motifs catered for by using a sufficiently large finite cluster. From a computational point of view, an advantage of using a cluster approach is that it is relatively unproblematic to accommodate large adsorbates. Periodic calculations would have an intrinsic advantage in automatically providing continuous substrate bands suitable to model the electronic structure of large nanocrystals. In periodic calculations, however, large adsorbates often require the use of very large unit cells in order to avoid undesired interactions across the periodic cell boundaries.

The current work is part of a combined experimental and theoretical investigation of the ultrafast photoinduced electron transfer of a series of perylene derivatives attached to nanostructured TiO_2 through a series of different anchor-cum-spacer groups.[39,40] The lack of spectral overlap of the absorption spectra of the ground-, excited-, and charge-separated states of perylene−TiO_2 interfaces makes it ideal for pump−probe spectroscopic investigations of the fundamental processes involved in photoinduced heterogeneous electron transfer.[16] As a purely organic chromophore attached to TiO_2 via a single anchor group, perylene is also a good candidate for quantum chemical calculations. This system therefore offers exceptionally good opportunities to make direct comparisons between experimental and calculated properties. In this paper we focus on calculated electronic structure properties and the ability to predict heterogeneous electron-transfer rates from first principles density functional calculations.

2. Method

2.1. Electronic Structure Calculations. The properties of the Pe, Pe−COOH, Pe−CH_2−CH_2−COOH, and Pe−CH═CH−COOH molecules, shown in Figure 2, were studied using the B3LYP hybrid functional and the standard 6-31G-(d,p) basis set in the Gaussian03 program.[41] Geometries were fully optimized, and the delocalization of the chromophore HOMO and LUMO orbitals into the anchor-cum-spacer groups was investigated. The S0→S1 excitation was investigated using time-dependent DFT (TD-DFT) calculations with the same functional and basis set. TD-DFT calculations typically give excitation energies accurate to a few tens of an eV for the lowest energy valence excitations at moderate computational cost.[42] There is a danger of spurious low energy excitation energies for charge transfer states due to incorrect treatment of self-interactions when applying TD-DFT to extended systems.[43] TD-DFT calculations have, however, been used successfully to investigate excitations in polycyclic aromatic molecules such as unsubstituted perylene,[44] and the approach appears to work well in the cases where the lowest valence excitations do not have strong charge-transfer character.

For the calculations of sensitized nanocrystals, a $(TiO_2)_{60}$ cluster fulfilling the recently suggested requirements of a

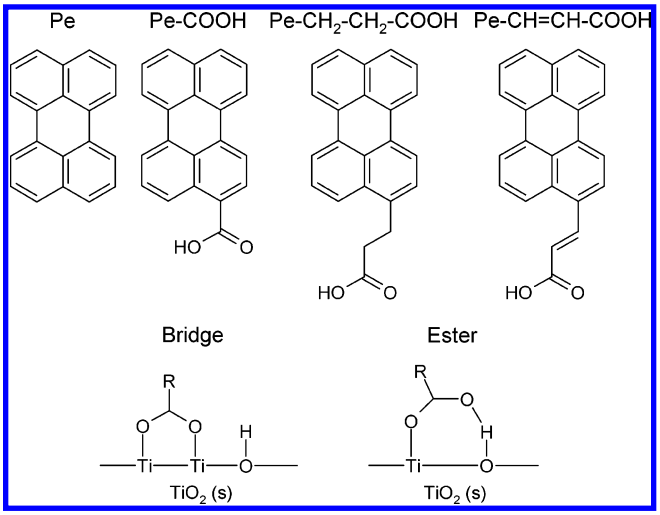

Figure 2. Investigated perylene (Pe) derivatives and surface binding modes. The investigated molecules are perylene (Pe), perylene with formic acid (Pe−COOH), propionic acid (Pe−CH_2−CH_2−COOH), and acrylic acid (Pe−CH═CH−COOH) anchor-cum-spacer groups. The carboxylic acid anchor group was considered to bind to the TiO_2 nanocrystal in a 2M-bidentate (bridge) fashion. For Pe−COOH, binding to the TiO_2 in molecular 1M-monodentate (ester) fashion was also considered.

nanocrystal was used.[38] Briefly, it has been found that neutral, stoichiometric clusters down to approximately 1 nm in diameter constructed so as to accommodate high coordination of all atoms (compatible with their formal oxidation states), and having a small or vanishing dipole moment, display significant structural stability and a well developed band structure.[38] Geometry optimizations of the here investigated systems were performed using DFT calculations with the PW86 exchange functional and the PW91 correlation functional together with a Slater Type Orbital (STO) Valence Single-Zeta (VSZ) basis set and large frozen cores as implemented in the ADF program.[45] This method combination is in the following referred to as PW/VSZ. The local structure of the interface between the TiO_2 nanoparticle and the various sensitizers were optimized at the same level of theory using a smaller $(TiO_2)_5(H_2O)_5$ cluster model. The different sensitizers were optimized on this cluster with relaxation of the local surface environment including the substrate atoms in the vicinity of the adsorbate, while keeping the saturating H_2O as well as the fringe atoms of the substrate cluster fixed. This stepwise optimization approach allows the reconstruction of supramolecular models with optimized adsorbates on optimized nanocrystals, including local relaxation of the nanocrystal in the vicinity of the adsorbate, at an affordable computational cost. It can be noted that water molecules are only used in order to saturate the small cluster used to optimize the adsorbate position on the substrate, and not the large nanocrystal. They are necessary in the small cluster model to saturate unphysical dangling bonds not present in the large nanocrystal which, as described above, has a sufficiently high coordination of every atom to ensure a reasonable description of the effective electronic band structure.[38] To further investigate the influence of the anchor group, a model system was constructed with an unsubstituted

perylene molecule (Pe) placed in the same position relative to the TiO_2 nanocrystal as in the optimized planar bridge binding case. As the aim was to compare the calculated electronic properties with and without anchor groups, rather than the interaction of a physisorbed perylene with a TiO_2 nanocrystal per se, this structure was based on the separately optimized parts without further optimization.

The electronic structure of the combined system was subsequently calculated with B3LYP using a split-valence basis set with large Effective Core Potentials (ECPs) using Gaussian03.[41] In these calculations, all atoms have a Gaussian Type Orbital (GTO) Valence Double-Zeta (VDZ) basis set, except oxygen which has a Valence Triple-Zeta (VTZ) basis set in order to allow a realistic representation of the negative ions in the nanocrystal. This particular method combination is referred to as B3LYP/VD(T)Z in the following and has been used in several previous investigations with good results to describe the electronic structure of systems comprising organic adsorbates on TiO_2 surfaces.[22,27] The B3LYP/VD(T)Z electronic structure calculations on PW/VSZ optimized geometries are referred to as B3LYP/VD(T)Z// PW/VSZ. As the electronic properties are more sensitive to the size of the basis set compared to the structural ones, the combination of a relatively small basis set for the optimizations together with a larger basis set for single point calculations of the electronic structure has been shown to offer a viable computational approach for these complex systems.[27] The basis set used here has, in particular, been used with good results for both structural and electronic properties in previous investigations of organic adsorbates on TiO_2 substrates.[22,27] Of particular relevance to the present application is that, as discussed previously,[22,27] this level of theory gives a reasonable calculated band structure of the TiO_2 substrate. A more detailed investigation of the structural and electronic properties of pure TiO_2 nanocrystals is underway and will be presented in due course.

2.2. Analysis of Interfacial Electronic Interaction. The solution to the time dependent Schrödinger equation has previously been calculated for the system under study assuming a constant value for the electronic coupling strength that reproduces the experimental time scale.[20] The time dependent pump−probe signal shows a monoexponential decay independent of the assumed strength for the electronic coupling as long as the molecular donor state is positioned high enough above the bottom of the empty conduction band of the semiconductor (wide band limit). In the latter case the decay behavior is virtually identical to that predicted by the Fermi's Golden rule perturbation treatment even though there is no restriction on the strength of the electronic coupling. This is not valid any more when the molecular donor level shifts closer to the conduction band edge. The validity of the wide band limit for the perylene chromophore and anatase or rutile TiO_2 has been confirmed experimentally with UPS and 2PPE measurements.[39,40]

Here, we consider the photoinduced surface electron transfer process based on evidence from explicit electronic structure calculations. The initial photoexcitation primarily involves exciations from the Highest Occupied Molecular Orbital (HOMO) to the Lowest Unoccupied Molecular Orbital (LUMO) on the perylene chromophore. The HOMO level, loosely corresponding to the perylene ground state, lies energetically in the band gap region of the TiO_2, as illustrated schematically in Figure 1. Although its energy may be shifted when it is adsorbed on the surface, the electronic interaction with the substrate is believed to be weak. This makes it readily identifiable as a single molecular level in an energy diagram, with a negligible broadening. The LUMO levels of all the chemically anchored sensitizers, on the other hand, are expected to show significant interaction with the conduction band, manifested in the splitting of the isolated sensitizer LUMO to a number of mixed sensitizer-semiconductor levels upon adsorption. According to the Newns-Anderson model for adsorbates on surfaces,[46] the effect of the adsorption on a molecular electronic level, i, is characterized by an energy shift, ΔE_i, relative to its gas-phase value, $E_i(\mathrm{g})$, and a lifetime broadening, $\hbar\Gamma_i$. The shift in energy is related to the gas-phase value by

$$E_i(\mathrm{ads}) = E_i(\mathrm{g}) + \Delta E_i \tag{1}$$

The lifetime broadening is described by a Lorentzian distribution that results from the decay of the excited molecular state resonantly coupled to a continuum of final, charge-separated, states.[47]

A detailed analysis of the electronic structure is necessary in order to quantify both the energy shift and broadening. In an attempt to quantify this interaction, a numerical fitting procedure of the Projected Density of States (PDOS) contributions has been implemented. First, an energy interval was selected within which the adsorbate PDOS contributions were considered to belong to the sensitizer LUMO. The interval was selected so that the PDOS contributions within this interval summed to one orbital. Generally this condition could be achieved to within 2%. This approach can only be expected to work in cases, such as this, where the considered orbital contributions are well separated in energy from those of other molecular orbitals. In more complicated cases, it will be necessary to use a more sophisticated approach involving orbital projection schemes to separate the different contributions. For the selected energy range, the calculated orbital energies, ϵ_i, of the combined system were weighted by the PDOS contributions, p_i, to obtain a weighted average calculated energy, $E_{\mathrm{LUMO}}(\mathrm{ads})$. Specifically, a molecular orbital, ψ_i, is expressed as a linear combination of n atomic orbitals, χ_j^A, centered on atom A, and with expansion coefficients c_{ij}^A:

$$\psi_i = \sum_j^n c_{ij}^A \chi_j^A \tag{2}$$

The portion of the orbital located on the adsorbate is taken to be p_i, which is given by the sum of the squares of the atomic orbital coefficients that are located on the adsorbate (ads) atoms.

$$p_i = \sum_j^{A\in\mathrm{ads}} (c_{ij}^A)^2 / \sum_j^n (c_{ij}^A)^2 \tag{3}$$

The inclusion of the denominator in eq 3 ensures that the probability is properly normalized. This is used to overcome potential complications associated with the fact that the atomic orbitals do not form an orthonormal set and that the sum of the coefficients squared is not strictly one. More stringent assignments would be possible, e.g. by taking the overlap matrix into account, but we have not found such a procedure necessary here.

We take the position of the adsorbate LUMO level in the combined system to be given by the weighted average:

$$E_{\mathrm{LUMO}}(\mathrm{ads}) = \sum_i p_i \epsilon_i \tag{4}$$

Subsequently, quantitative measures of the width of the energy distribution of the LUMO contributions were sought from calculated mean deviation (MD) and root-mean-squared (RMS) values of the selected set of PDOS contributions

$$\hbar\Gamma_{\mathrm{MD}} = p_i|\epsilon_i - E_{\mathrm{LUMO}}(\mathrm{ads})| \tag{5}$$

$$\hbar\Gamma_{\mathrm{RMS}} = \sqrt{\sum_i p_i(\epsilon_i - E_{\mathrm{LUMO}}(\mathrm{ads}))^2} \tag{6}$$

To test the accuracy of the assignment of an effective width to a finite distribution of levels, sets of discrete peaks following a Lorentzian distribution were created and analyzed according to the scheme outlined above for a variety of initial line widths. The calculated MD and RMS line widths were both found to yield correct orders of magnitudes and trends for a wide range of discrete Lorentzian distributions, although the quality of the fit depended on the chosen line width and spacing. For a spacing of 20 meV (similar to that found in the $(TiO_2)_{60}$ cluster) and line widths in the 1−150 meV range, the MD analysis yielded calculated line widths that matched the true value to within 20%. Generally the MD analysis was found to underestimate stronger couplings. The RMS analysis was found to be somewhat less robust compared to the MD analysis, with a tendency to overestimate the line widths for small couplings but to be of similar quality or better than the MD results for line widths exceeding 150 meV. In the analysis below, we have used the MD line widths. It can be noted that these simple ways to approximate a broadening of a molecular level in the presence of a substrate band may in future applications be replaced by a direct fit of the adsorbate level distribution to a Lorentzian function.

The results of the line width-fittings are used to construct Lorentzian distributions, ρ_{LUMO}, with width $\hbar\Gamma$ centered at $E_{\mathrm{LUMO}}(\mathrm{ads})$.[46,47]

$$\rho_{\mathrm{LUMO}}(E) = \frac{1}{(E - E_{\mathrm{LUMO}}(\mathrm{ads}))^2 + \left(\frac{\hbar\Gamma}{2}\right)^2} \tag{7}$$

Finally, the ability of the calculated energy broadenings to capture essential features of the electronic coupling, in the wide band limit of heterogeneous electron-transfer encountered here, was considered by using the calculated PDOS broadenings as an effective measure of an electronic coupling strength that can be converted to an electron-transfer time according to[46,47]

$$\tau = \hbar/\hbar\,\Gamma \tag{8}$$

In convenient numerical units this becomes

$$\tau(\mathrm{fs}) = 658/\Gamma(\mathrm{meV}) \tag{9}$$

3. Results

3.1. Molecular Properties. Molecular properties of the substituted perylenes were first investigated using the standard B3LYP/6-31G(d,p) methodology. In particular, the S0→S1 excitation that is responsible for the photoinduced charge-separation was investigated. This excitation is dominated by the promotion of an electron from the perylene HOMO to the perylene LUMO orbital.[44] The HOMO and LUMO molecular orbitals for the four different molecules are shown in Figure 3. The results for the unsubstituted perylene molecule are similar to those published by Halasinski et al.[44] For all substituents, both the HOMO and LUMO orbitals are delocalized π orbitals. The HOMO orbitals of all the different systems are, moreover, very similar to the HOMO orbital of the unsubstituted perylene molecule, with essentially negligible contributions on the anchor-cum-spacer groups. The LUMO orbital of Pe−CH_2−CH_2−COOH is also very similar to that of the unsubstituted perylene, consistent with the notion that the saturated spacer group is a poor mediator of electron delocalization. The Pe−COOH and Pe−CH═CH−COOH molecules, on the other hand, show considerable delocalization of the perylene LUMO orbital into the anchor-cum-spacer moiety. Interestingly, this is in both cases accompanied by a reorganization of the perylene π* part of the orbital, compared to its symmetrical appearance in perylene itself, in such a way that the perylene π* orbital is located to a larger extent in the vicinity of the substituent. In Pe−COOH, the LUMO orbital can be recognized as a bonding combination between the first perylene π* orbital with the first carboxylate π* orbital. In the Pe−CH═CH−COOH molecule, the LUMO orbital is seen to be essentially a bonding combination of the first π* orbitals of each of the individual parts of the chromophore-spacer-anchor system. It is noteworthy that the delocalization across the unsaturated spacer is sufficiently effective for the anchor group π* to carry nearly equal weight to the LUMO as in the Pe−COOH system. Such delocalizations are consistent with facilitated electron transfer across the anchor-cum-spacer unit.[8,25]

3.2. Molecular Excited States. The vertical excitation energies for the S0 → S1 transition has been calculated using TD- B3LYP/6-31G(d,p) for the various anchor-cum-spacer groups. The results are listed in Table 1. The excitation is in all cases dominated by the HOMO−LUMO transition with no significant charge-transfer character. This means that the LUMO delocalization discussed above is reflected also in the electron distribution of the S1 state, giving further support to the notion that the delocalization of the LUMO facilitates interfacial electron injection. The Pe−COOH and Pe−CH═CH−COOH cases that showed the largest delocalization of the LUMO also show a significant red-shift of the absorption of 0.2 and 0.3 eV, respectively. Twisting the plane of the

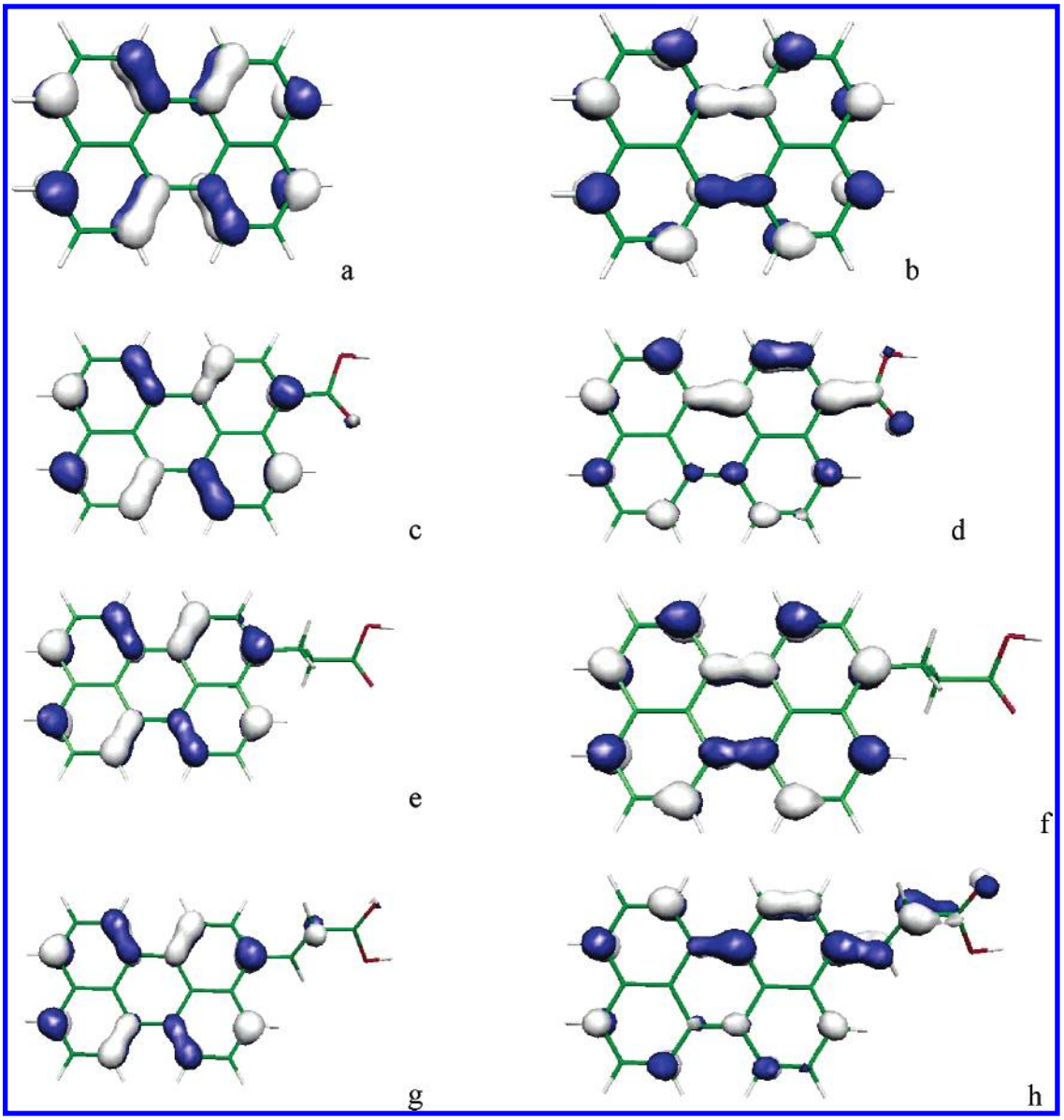

Figure 3. HOMO (left column) and LUMO (right column) orbitals of Pe (a,b), Pe−COOH (c,d), Pe−CH_2−CH_2−COOH (e,f), and Pe−CH=CH−COOH (g,h) according to B3LYP/6-31G(d,p) calculations.

Table 1. Vertical S0→S1 Exciation Energies of Perylenes with Different Anchor-Cum-Spacer Groups, Calculated Using Time Dependent B3LYP/6-31G(d,p)[a]

molecule	*E*/eV	λ/nm	*f*	excitation
Pe	2.89	428.4	0.36	0.62(HOMO→LUMO) −0.11(HOMO-4→ LUMO+2)
Pe−COOH	2.69	461.0	0.40	0.62(HOMO→LUMO)
Pe−CH_2−CH_2−COOH	2.85	435.2	0.43	0.62(HOMO→LUMO)
Pe−CH=CH−COOH	2.60	477.5	0.57	0.62(HOMO→LUMO)

[a] The excitation energies, *E*, wavelengths, λ, oscillator strengths, *f*, and main contributions (excitation coefficients > 0.1) are included in the table.

carboxylate anchor group 90 degrees relative to the perylene plane in Pe−COOH results in a decoupling of carboxylate and perylene π orbitals and a reduction of the red-shift in the absorption compared to the pure perylene case. The injection rates can thus be expected to be sensitive to the detailed structure of the adsorbed chromophore, as already suggested for the isonicotinic acid model chromophore.[27] Furthermore, if the shifts are sufficiently large to be observable spectroscopically, they can serve as a sensitive probe for the local geometry once any adsorption-induced shifts have been taken into account.

3.3. Geometry of the Sensitized Nanocrystals. Atomistic models for the various sensitizers bound to a TiO_2 nanocrystal were constructed from a common, fully optimized, $(TiO_2)_{60}$ cluster. The sensitizer geometries as well as local substrate relaxations in the vicinity of the adsorption site were obtained from geometry optimizations of the sensitizers on a smaller $(TiO_2)_5(H_2O)_5$ cluster. The initial geometry of the smaller cluster was taken from a prototypical anatase (101) surface region of the full $(TiO_2)_{60}$ cluster. To combine a consistent treatment of the sensitized $(TiO_2)_5(H_2O)_5$ and $(TiO_2)_{60}$ clusters, with local surface relaxation near the adsorption site, the atoms at the perimeter of the $(TiO_2)_5$-$(H_2O)_5$ cluster were saturated by hydrogen atoms or hydroxyl groups. The edge atoms together with the hydrogen and

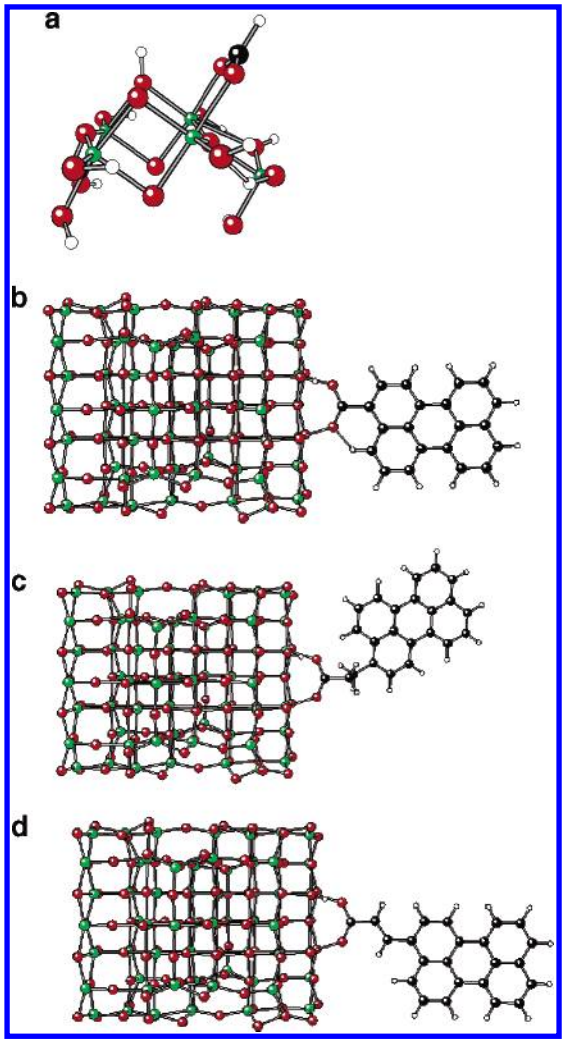

Figure 4. Optimized geometries of sensitized titanium dioxide clusters: (a) HCOOH−$(TiO_2)_5(H_2O)_5$, (b) bridge-binding, planar Pe−COOH−$(TiO_2)_{60}$, (c) Pe−CH_2−CH_2−COOH−$(TiO_2)_{60}$, and (d) Pe−CH═CH−COOH−$(TiO_2)_{60}$. Note that the proton from the carboxylic acid has been transferred to a surface oxygen in the bridge binding mode displayed in 1b−d, in accordance with the bridge binding scheme in Figure 2.

hydroxyl saturators were kept fixed during the subsequent optimization, while the sensitizer and the $(TiO_2)_5(H_2O)_5$ cluster atoms in the vicinity of the adsorption site were fully optimized. Finally, the locally optimized small cluster models were reintroduced into the framework of the large cluster. The geometries of carboxylic acid anchored to the $(TiO_2)_5$-$(H_2O)_5$ cluster and the three combined sensitizer-$(TiO_2)_{60}$ clusters are shown in Figure 4. The PW/VSZ optimized structures agree well with the results of published information about the binding of carboxylic acids to anatase TiO_2 surfaces.[48,49] However, for a nanocrystal such as the $(TiO_2)_{60}$ cluster used here, there are a large number of local adsorption sites with different absorption possibilities. As the present paper focuses on the electronic aspects of the interfaces, we have not tried to find the overall most favorable adsorption site on the nanocrystal. The selected adsorption site should instead only be viewed as a typical surface site, for which we have investigated the effect of the binding on the electronic properties by optimizing both an ester and a bridge binding carboxylic acid, see Figure 2. These two modes are both favorable on TiO_2, and it is not unreasonable to assume that they will either exist in parallel or that the detailed experimental conditions will determine which binding mode prevails. Although beyond the scope of the present paper, more systematic investigations of the binding of anchor groups to nanocrystals, for example comparing different surface sites, investigating the dependence of the size and shape of the nanocrystal, and making comparisons to the binding on surfaces, are interesting and underway.

3.4. Electronic Structure of the Sensitized Nanocrystals. The electronic structures of the combined sensitizer-nanocrystal systems were calculated at the B3LYP/VD(T)Z//PW/VSZ level. An effective total Density of States (DOS) was in each case constructed from the calculated orbital energies using an arbitrary Gaussian broadening of 0.3 eV, and the results are shown in Figure 5. The sensitizer contributions to this DOS have also been extracted using the appropriate atomic orbital coefficients. These contributions are shown in Figure 5 as the 0.3 eV broadened PDOS. Due to the large number of substrate atoms, the total DOS is in all cases dominated by the $(TiO_2)_{60}$ cluster contributions. The calculated DOS is thus very similar for all the studied systems and is only shown as a whole for the nonbound Pe-$(TiO_2)_{60}$. The total DOS spectra display a completely occupied valence band below ca. −7 eV and a completely empty conduction band above ca. −4 eV. The valence and conduction band energies are in all cases within 0.5 eV of the −7.25 and −3.54 eV values calculated for the valence and conduction band edges of an unsensitized $(TiO_2)_{60}$ nanocrystal, respectively. This indicates that the $(TiO_2)_{60}$ cluster model gives a robust and realistic representation of the TiO_2 band gap, both compared to experiment[3] and to periodic TiO_2 calculations using the B3LYP functional with a similar basis set.[27]

The sensitizer contributions to the electronic structure, in the region of interest for the photoexcitation processes involving the chromophore ground and first excited states, can be seen by focusing on the adsorbate PDOS, which are shown in Figure 5 with a magnification of the *y*-axis by a factor of 10 compared to the total DOS for all the different systems. The perylene HOMO π orbital is in all cases easily recognized as a single level located in the band gap region at ca. −6 eV. The LUMO π^* orbital is distributed into a number of contributions to mixed molecule-semiconductor levels around −3 eV. This is about 0.5 eV above the conduction band edge, indicating that heterogeneous electron transfer is energetically possible from the sensitizer LUMO orbital involved in the first excited sensitizer state which was shown earlier to be dominated by a HOMO−LUMO excitation.

3.5. Electronic Coupling Strength. The electronic coupling strength governing the photoinduced heterogeneous electron transfer is likely to be determined largely by the interactions between the sensitizer LUMO orbital and the substrate conduction band. To investigate this interaction more thoroughly, we have made a detailed investigation of the adsorbate LUMO PDOS. The results for the various sensitizers are shown in Figure 6. The figure clearly shows that the calculations predict that the investigated systems

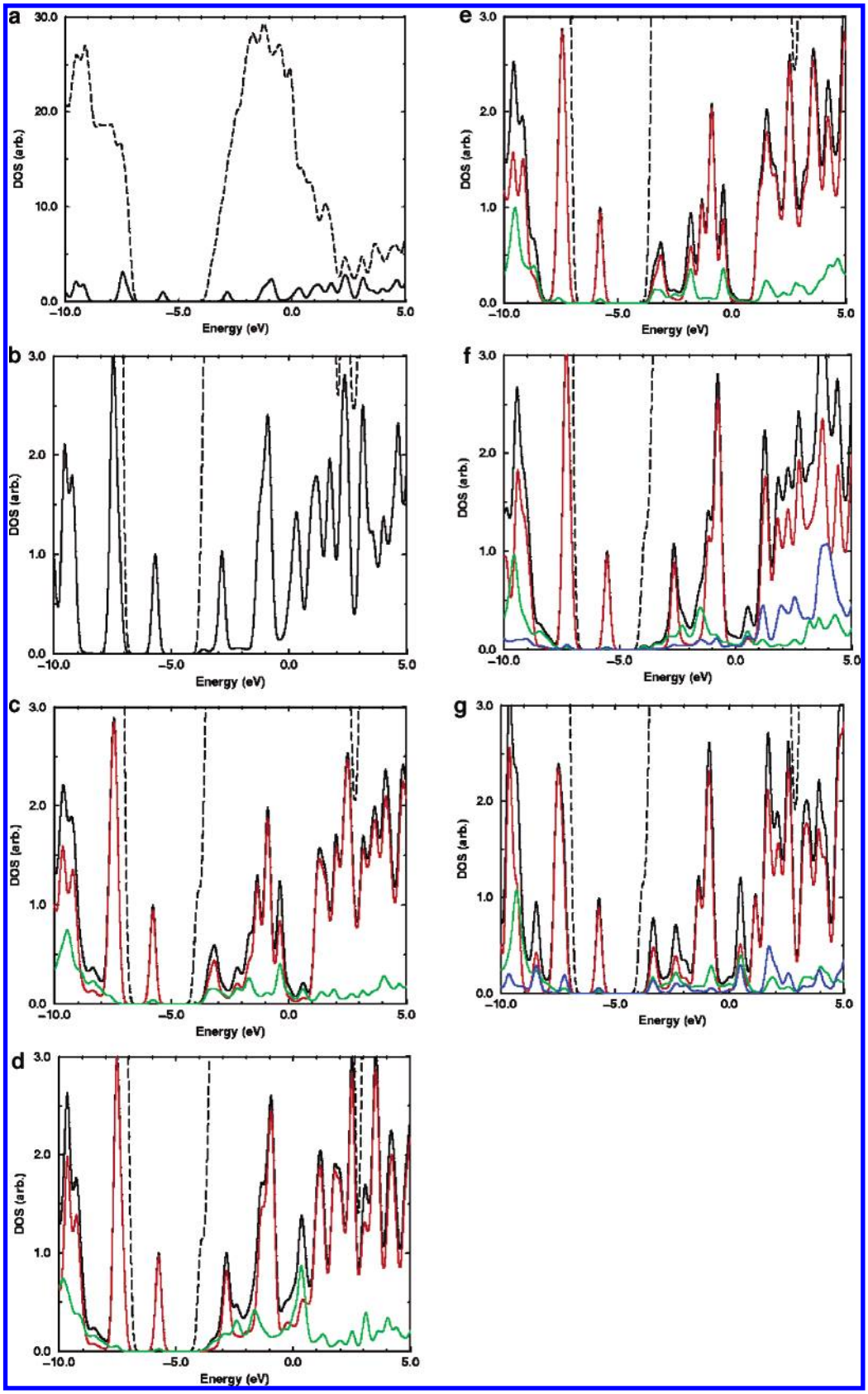

Figure 5. Total and projected DOS plots of the sensitizer-nanocrystal systems. The different panels show (a) Pe−$(TiO_2)_{60}$ DOS, (b) Pe−$(TiO_2)_{60}$ adsorbate PDOS, (c) Pe−COOH−$(TiO_2)_{60}$ adsorbate PDOS for planar bridge adsorption, (d) Pe−COOH−$(TiO_2)_{60}$ adsorbate PDOS for twisted bridge adsorption, (e) Pe−COOH−$(TiO_2)_{60}$ adsorbate PDOS for planar ester adsorption, (f) Pe−CH_2−CH_2−COOH−$(TiO_2)_{60}$ adsorbate PDOS, and (g) Pe−CH═CH−COOH−$(TiO_2)_{60}$ adsorbate PDOS. In all cases: dashed line − total DOS, black line − total adsorbate PDOS, red line − Pe PDOS, green line − COO PDOS, blue line − spacer group PDOS. The DOS and PDOS plots rely on an arbitrary 0.3 eV Gaussian broadening of the calculated orbital energies, used to facilitate visual comparisons.

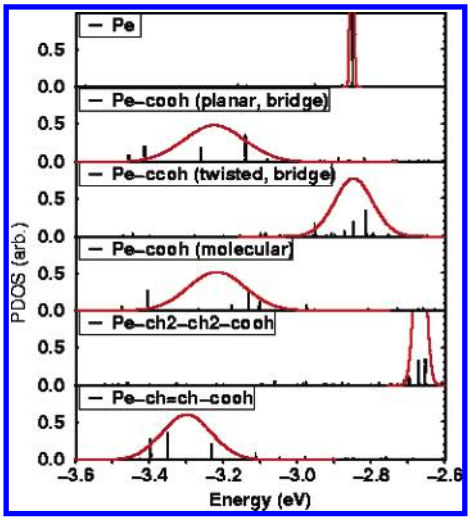

Figure 6. LUMO PDOS plots for the substituted perylenes on $(TiO_2)_{60}$. Black lines − sensitizer orbital (PDOS) contributions. Red curves − Lorentzian fitted curves, ρ_{LUMO}, with parameters from Table 2. To facilitate visual comparison between the PDOS and the Lorentzian curves, the heights of the curves have been scaled so that a curve with a 100 meV fwhm has a height of 0.5.

differ both in the exact position of the LUMO level and the degree to which the sensitizer LUMO orbital mixes with the substrate conduction band. A more detailed analysis is possible from a consideration of the results of the MD-fittings described in section 2.2 of the sensitizer LUMO broadening which are presented in Table 2 and represented graphically in Figure 6 as Lorentzian distributions, ρ_{LUMO}, with width $\hbar\Gamma$ centered at E_{LUMO}(ads). Although the PDOSs obtained from the electronic structures consist of a finite number of states which do not generally follow a simple Lorentzian distribution, visual comparison of the fitted functions with the plot of the individual PDOS contributions in Figure 6 indicates that the fitting successfully captures trends in terms of both energy shifts and broadenings.

The electron-transfer times estimated from the analysis of the quantum chemical calculations fall in the femtosecond time range and are compared with experimental values in Table 2. The listed experimental values were obtained from a monoexponential fit to the measured rise of the molecular product state, i.e., the ionized perylene chromophore, which was monitored as characteristic absorption signal in a femtosecond laser pump−probe experiment. The experiments were carried out with cross-correlation signals of below 25 fs width (fwhm). The perylene dyes were adsorbed from solution on the inner surface of nano-structured anatase TiO_2 layers of about 2 micrometer thickness. The measurements were carried out in ultrahigh-vacuum. Further details are described in a recent Ph.D. thesis by R. Ernstorfer.[39] A very similar trend, with very similar absolute values for the injection times of the same perylene dyes, was measured even more recently applying the technique of femtosecond two-photon photoemission. In the latter case the same perylene dyes were adsorbed but on the (110) surface of a rutile TiO_2 single crystal. Details of these measurements can be found in a recent Ph.D. thesis by L. Gundlach.[40]

As seen in Table 2, the theoretically estimated injection times for the three systems where a direct comparison can be made with experimental measurements are of the right order of magnitude, with τ_{calc} up to a factor of 2 faster than τ_{exp} in all three cases. As the discrepancy between theory and experiment is systematic between the investigated systems, the agreement in terms of the relative injection times is better than in terms of absolute rates. In particular, the calculations predict that the introduction of the saturated ($-CH_2-CH_2-$) spacer slows down the injection by about a factor of 5 compared to the Pe−COOH case, while the corresponding introduction of the unsaturated ($-CH=CH-$) spacer leaves the injection time essentially unaltered. This is in good agreement with the experimental ratios of 4.3 and 0.8, respectively.

The results for the nonbound Pe−$(TiO_2)_{60}$ structure show that without the presence of the anchor group the electronic coupling is reduced substantially. The LUMO of the pure perylene is concentrated almost entirely to a single molecular level at −2.85 eV. This constitutes a significantly weaker coupling compared to all the anchored chromophores. Comparing with the twisted bridge situation, the presence of the anchor group therefore seems to play an important role in enhancing the interfacial electronic coupling also when it is not directly involved in delocalization of the donor level.

There are a number of factors that can influence the calculated absolute injection times. This includes both purely computational effects and discrepancies between the calculated and experimental systems. In terms of the calculations, more work is needed to test the performance of different density functional methods, and basis set effects. Another potential source of error is that it is assumed in the

Table 2. Electronic Interactions between the First Unoccupied Sensitizer Level (LUMO) and the TiO_2 Conduction Band for Systems with Different Anchor-Cum-Spacer Groups and Adsorption Modes[a]

sensitizer	adsorption mode	E_{LUMO}(ads)/ eV	$\hbar\Gamma_{calc}$/ meV	τ_{calc}/ fs	τ_{exp}/ fs
Pe	nonbound	−2.85	2	330	NA
Pe−COOH	planar bridge	−3.22	139	5	13
Pe−COOH	twisted bridge	−2.85	68	10	
Pe−COOH	ester	−3.22	140	5	
Pe−CH_2−CH_2−COOH	bridge	−2.67	20	33	57
Pe−CH=CH−COOH	bridge	−3.30	102	6	10

[a] The table includes the position of the sensitizer LUMO level in the combined system as the weighted average energy, E_{LUMO}(ads), the calculated effective broadening of the level, $\hbar\Gamma_{calc}$, due to the interaction with the surface from the MD analysis described in the text as well as calculated and experimental heterogeneous electron-transfer times.

calculations that electron transfer occurs from the LUMO, whereas in the actual experiment electron transfer occurs from the excited electronic singlet state of perylene. Correspondingly, the energy shifts calculated for the LUMO when the perylene chromophore is attached to the different anchor-cum-spacer groups cannot be seen with the same magnitude for the excited state as is borne out by the absorption spectra and also by the UPS and 2PPE measurements probing the energy of the excited singlet state of the perylene chromophore with respect to the lower edge of the conduction band of the semiconductor TiO_2.[39,40] Dynamic effects could also contribute to the discrepancy, and the optimized geometries used in the present calculations may, in fact, correspond to geometries where the LUMOs are more strongly coupled to the substrate conduction band compared to the average value during the thermal and vibrational motion of the system. In terms of the compatibility with the experimental system, the present calculations assume an ideal surface termination, with direct chemical bonding from the anchor group to substrate Ti atoms. If the experimental systems are not atomically clean, such direct bonding could be prevented for some fraction of the dye molecules. Sample contamination is therefore also a potential source for a systematic weakening of the interfacial electronic coupling.

4. Conclusions

A series of perylene-sensitized TiO_2 nanoparticles has been studied theoretically from first principles using density functional theory calculations. Calculated electronic properties have been directly compared to experimental information about heterogeneous electron-transfer rates in the femtosecond time regime. Calculated approximate heterogeneous electron-transfer rates agree with the experimental values to within a factor of 2, and the trends for relative rates are found to agree well with the experimental results. This suggests that this kind of supramolecular calculation of dye molecules on nanoparticles can be used to predict how changes to the structure or composition of dye-sensitized semiconductor systems will affect their ultrafast electron-transfer properties. As there are no problems to accommodate larger adsorbates in the cluster approach, we believe that this approach will prove to be very useful for studies of large heterosupramolecular systems containing both organic and organometallic photo- and redox-centers attached to semiconductor nanoparticles.

Acknowledgment. The Göran Gustafsson Foundation and the Magnus Bergvall Foundation are gratefully acknowledged for financial support. We also thank the Swedish National Supercomputer Center (NSC) for generous allocations of computer resources. P.P. and M.J.L. acknowledges Prof. Sten Lunell, Uppsala University, and Dr. Lars Ojamäe, Linköping University, for stimulating discussions.

References

(1) Miller, R. J. D.; McLendon, G. L.; Nozik, A. J.; Schmickler, W.; Willig, F. *Surface Electron Transfer Processes*; VCH Publishers: 1995.

(2) Kavarnos, G. J. *Fundamentals of Photoinduced Electron Transfer*; VCH Publishers: 1993.

(3) Hagfeldt, A.; Grätzel, M. *Chem. Rev.* **1995**, *95*, 49.

(4) Hagfedt; A.; Grätzel, M. *Acc. Chem. Res.* **2000**, *33*, 269.

(5) O'Regan, B.; Grätzel, M. *Nature* **1991**, *353*, 737.

(6) Kalyanasundadaram, K.; Grätzel, M. *Coord. Chem. Rev.* **1998**, *95*, 49.

(7) Galoppini, E. *Coord. Chem. Rev.* **2004**, *248*, 1161.

(8) Schnadt, J. et al. *Nature* **2002**, *418*, 620.

(9) Zimmermann, C.; Willig, F.; Ramakrishna, S.; Burfeindt, B.; Pettinger, B.; Eichberger, R.; Storck, W. *J. Phys. Chem. B* **2001**, *105*, 9245.

(10) Benkö, G.; Kallioinen, J.; Korppi-Tommola, J. E. I.; Yartsev, A.; Sundström, V. *J. Am. Chem. Soc.* **2002**, *124*, 489.

(11) Huber, R.; Moser, J. E.; Grätzel, M.; Wachtveitl, J. *J. Phys. Chem. B* **2002**, *106*, 6494.

(12) Asbury, J. B.; Hao, E.; Wang, Y.; Lian, T. *J. Phys. Chem. B* **2001**, *105*, 4545.

(13) Marcus, R. A.; Sutin, N. *Biochim. Biophys. Acta* **1985**, *811*, 265.

(14) Lanzafame, J. M.; Palese, S.; Wang, D.; Miller, R. J. D.; Muenter, A. A. *J. Phys. Chem.* **1994**, *98*, 11020.

(15) Marcus, R. A. *J. Chem. Phys.* **1965**, *43*, 679.

(16) Willig, F.; Zimmermann, C.; Ramakrishna, S.; Storck, W. *Electrochim. Acta* **2000**, *45*, 4565.

(17) *Topics in Current Chemistry;* Gerischer, H., Willig, Boschke, F. F. L., Eds.; Springer: Berlin, 1976; Vol. 61, p 31.

(18) Newton, M. D. *Chem. Rev.* **1991**, *91*, 767.

(19) Adams, D. M. et al. *J. Phys. Chem. B* **2003**, *107*, 668.

(20) Ramakrishna, S.; Willig, F.; May, V.; Knorr, A. *J. Phys. Chem. B.* **2003**, *107*, 607.

(21) Wang, L. X.; Ernstorfer, R.; Willig, F.; May, V. *J. Phys. Chem. B* **2005**, *109*, 9589.

(22) Persson, P.; Bergström, R.; Ojamäe, L.; Lunell, S. *Adv. Quantum Chem.* **2002**, *41*, 203.

(23) Persson, P.; Stashans, A.; Bergström, R.; Lunell, S. *Int. J. Quantum Chem.* **1998**, *70*, 1055.

(24) Persson, P.; Lunell, S. *Sol. Energy Mater. Sol. Cells* **2000**, *63*, 139.

(25) Persson, P. et al. *J. Chem. Phys.* **2000**, *112*, 3945.

(26) Persson, P.; Bergström, R.; Lunell, S. *J. Phys. Chem. B* **2000**, *104*, 10348.

(27) Persson, P.; Lunell, S.; Ojamäe, L. *Chem. Phys. Lett.* **2000**, *364*, 469.

(28) Stier, W.; Prezhdo, O. V. *J. Phys. Chem. B* **2002**, *106*, 8047.

(29) Redfern, P. C.; Zapol, P.; Curtiss, L. A.; Rajh, T.; Thurnauer, M. C. *J. Phys. Chem. B* **2003**, *107*, 11419.

(30) Rego, L. G. C.; Batista, V. S. *J. Am. Chem. Soc.* **2003**, *125*, 7989.

(31) Stier, W.; Duncan, W. R.; Prezhdo, O. V. *Adv. Mater.* **2003**, *16*, 240.

(32) De Angelis, F.; Tilocca, A.; Selloni, A. *J. Am. Chem. Soc.* **2004**, *126*, 15024.

(33) Persson, P.; Lundqvist, M. J. *J. Phys. Chem. B* **2005**, *109*, 11918.

(34) Vega-Arroyo, M.; LeBreton, P. R.; Rajh, T.; Zapol, P. Curtiss, L. A. *Chem. Phys. Lett.* **2005**, *406*, 306.

(35) Rego, L. G. C.; Abuabara, S. G.; Batista, V. S. *J. Chem. Phys.* **2005**, *122*, 154709.

(36) Noguera, C *Surf. Rev. Lett.* **2001**, *8*, 121.

(37) Bredow, T.; Jug, K. *J. Phys. Chem.* **1995**, *99*, 285.

(38) Persson, P.; Gebhardt, J. C. M.; Lunell, S. *J. Phys. Chem. B* **2003**, *107*, 3336.

(39) Ernstorfer, R. Spectroscopic investigation of photoinduced heterogeneous electron transfer, Ph.D. Thesis, Freie Universität Berlin, Germany, 2004.

(40) Gundlach, L. Surface Electron-Transfer Dynamics in the Presence of Organic Chromophores, Ph.D. Thesis, Freie Universität Berlin, Germany 2005.

(41) *Gaussian 03, Revision C.02*; Frisch, M. J.; Trucks, G. W.; Schlegel, H. B.; Scuseria, G. E.; Robb, M. A.; Cheeseman, J. R.; Montgomery, J. A., Jr.; Vreven, T.; Kudin, K. N.; Burant, J. C.; Millam, J. M.; Iyengar, S. S.; Tomasi, J.; Barone, V.; Mennucci, B.; Cossi, M.; Scalmani, G.; Rega, N.; Petersson, G. A.; Nakatsuji, H.; Hada, M.; Ehara, M.; Toyota, K.; Fukuda, R.; Hasegawa, J.; Ishida, M.; Nakajima, T.; Honda, Y.; Kitao, O.; Nakai, H.; Klene, M.; Li, X.; Knox, J. E.; Hratchian, H. P.; Cross, J. B.; Bakken, V.; Adamo, C.; Jaramillo, J.; Gomperts, R.; Stratmann, R. E.; Yazyev, O.; Austin, A. J.; Cammi, R.; Pomelli, C.; Ochterski, J. W.; Ayala, P. Y.; Morokuma, K.; Voth, G. A.; Salvador, P.; Dannenberg, J. J.; Zakrzewski, V. G.; Dapprich, S.; Daniels, A. D.; Strain, M. C.; Farkas, O.; Malick, D. K.; Rabuck, A. D.; Raghavachari, K.; Foresman, J. B.; Ortiz, J. V.; Cui, Q.; Baboul, A. G.; Clifford, S.; Cioslowski, J.; Stefanov, B. B.; Liu, G.; Liashenko, A.; Piskorz, P.; Komaromi, I.; Martin, R. L.; Fox, D. J.; Keith, T.; Al-Laham, M. A.; Peng, C. Y.; Nanayakkara, A.; Challacombe, M.; Gill, P. M. W.; Johnson, B.; Chen, W.; Wong, M. W.; Gonzalez, C.; Pople, J. A. Gaussian, Inc.: Wallingford, CT, 2004.

(42) Koch, W.; Holthausen, M. *A Chemist*'s *Guide to Density Functional Theory*; Wiley-VCH: Weinheim, 2001.

(43) Dreuw, A.; Head-Gordon, M. *J. Am. Chem. Soc.* **2004**, *126*, 4007.

(44) Halasinski, T. M.; Weisman, J. L.; Ruiterkamp, R.; Lee, T. J.; Salama, F.; Head-Gordon, M. *J. Phys. Chem. A* **2003**, *107*, 3660.

(45) (a) te Velde, G.; Bickelhaupt, F. M.; van Gisbergen, S. J. A.; Fonseca Guerra, C.; Baerends, E. J.; Snijders, J. G.; Ziegler, T. *J. Comput. Chem.* **2001**, *22*, 931. (b) Fonseca Guerra, C.; Snijders, J. G.; te Velde, G.; Baerends, E. J. *Theor. Chem. Acc.* **1998**, *99*, 391. (c) Baerends, E. J.; Autschbach, J. A.; Bacrces, A.; Bo, C.; Boerrigter, P. M.; Cavallo, L.; Chong, D. P.; Deng, L.; Dickson, R. M.; Ellis, D. E.; Fan, L.; Fischer, T. H.; Fonseca Guerra, C.; van Gisbergen, S. J. A.; Groeneveld, J. A.; Gritsenko, O. V.; Graning, M.; Harris, F. E.; van den Hoek, P.; Jacobsen, H.; van Kessel, G.; Kootstra, F.; van Lenthe, E.; Osinga, V. P.; Patchkovskii, S.; Philipsen, P. H. T.; Post, D.; Pye, C. C.; Ravenek, W.; Ros, P.; Schipper, P. R. T.; Schreckenbach, G.; Snijders, J. G.; Sola, M.; Swart, M.; Swerhone, D.; te Velde, G.; Vernooijs, P.; Versluis, L.; Visser, O.; van Wezenbeek, E.; Wiesenekker, G.; Wolff, S. K.; Woo, T. K.; Ziegler, T. ADF2002.03, SCM, Theoretical Chemistry, Vrije Universiteit, Amsterdam, The Netherlands, http://www.scm.com.

(46) Muscat, J. P.; Newns, D. M. *Prog. Surf. Sci.* **1978**, *9*, 1.

(47) Cohen-Tannoudji, C.; Diu, B.; Laloe, F. *Quantum Mechanics;* J. Wiley and Sons: Paris, 1977; Vol. 2.

(48) Vittadini, A.; Selloni, A.; Rotzinger, F. P.; Grätzel, M. *J. Phys. Chem. B* **2000**, *104*, 1300.

(49) Diebold, U. *Surf. Sci. Reports* **2003**, *48*, 53.

CT050141X